ARTICLE

Hydrogen-Bond-Assisted Conformational Selection of Picaridin in the Gas Phase

Received 00th January 20xx,
Accepted 00th January 20xx

DOI: 10.1039/x0xx00000x

Otger Crehuet,[a,b] Andrea Vázquez,[a,b] Francisco J. Basterretxea,[a] Pablo Pinacho,*[,a,c] and Emilio J. Cocinero*[,a,b]

Understanding the intrinsic shape of bioactive molecules such as picaridin is key to elucidating their mode of action. In this work, we characterize the gas-phase conformational landscape of picaridin, a flexible chiral repellent with two stereocenters. Broadband rotational spectroscopy combined with quantum chemical calculations reveals a single dominant conformer per enantiomeric pair, both stabilized by internal O–H···O hydrogen bonds. These intramolecular interactions induce conformational locking, constraining the hydroxyethyl chain and favouring a compact geometry. Non-covalent interaction analysis further confirms that dispersion and hydrogen bonding play a central role in conformational selection under isolated conditions.

Introduction

Vector-borne diseases remain a major global health concern, and chemical insect repellents play a critical role in minimizing human–vector interactions.[1] Since the mid-20th century, considerable efforts have been devoted to developing synthetic repellents with improved volatility, longer-lasting effects, and enhanced safety compared to natural alternatives. These developments led to the introduction of molecules capable of disrupting insect host-seeking behaviour by interfering with olfactory receptors, ultimately reducing transmission of diseases such as malaria, dengue, and Zika.[2]

Modern synthetic repellents are characterized by their volatility and structural diversity. Their scaffolds incorporate a range of functional groups, including piperidines, diols, amides, esters, and terpenes.[3,4] Among them, *N,N*-diethyl-*m*-toluamide (DEET) and picaridin have emerged as the most widely used. While DEET has served as the historical benchmark for repellent efficacy, picaridin—also known as icaridin or KBR 3023—was developed more recently through ligand-based molecular design rooted in known bioactive frameworks.[5,6] Picaridin is currently recommended by major international agencies, including the World Health Organization (WHO) and the U.S. Centers for Disease Control and Prevention (CDC), owing to its broad-spectrum efficacy, low dermal absorption, and favourable toxicological and sensory profile. Its activity has been shown to rival or exceed that of DEET in both laboratory and field conditions.[7]

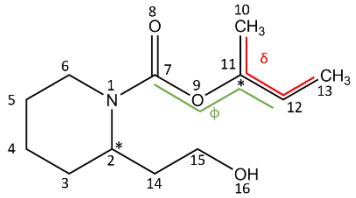

Figure 1. Structural formula of 1-(1-methylpropoxycarbonyl)-2-(2-hydroxyethyl)piperidine (picaridin), showing the atom numbering. The stereogenic centres (C2 and C11) are marked with asterisks (*).

Chemically, picaridin is a chiral carbamate derivative of piperidine (Figure 1), featuring a sec-butyl ester group at the nitrogen atom and a hydroxyethyl chain at the 2-position. The molecule contains two stereogenic centres, giving rise to four diastereomers grouped into two enantiomeric pairs: (*11R,2R*)/(*11S,2S*) and (*11R,2S*)/(*11S,2R*). Previous studies have identified the (*11R,2S*) diastereomer as the most biologically effective.[8] The presence of flexible alkyl chains and polar functional groups imparts considerable conformational freedom, which may influence the molecule's interaction with olfactory proteins and other biological targets. However, a detailed picture of picaridin's intrinsic conformational preferences remains elusive.

Most structural studies of picaridin have been performed in condensed phases, where intermolecular forces such as solvation and crystal packing can distort geometries and mask subtle intramolecular effects. In contrast, gas-phase studies allow access to unperturbed molecular structures and the intrinsic balance of internal interactions. High-resolution rotational spectroscopy, particularly when combined with supersonic jet cooling, offers an

[a.] *Departamento de Química Física, Facultad de Ciencia y Tecnología, Universidad del País Vasco (UPV/EHU), Leioa, 48940, Spain.*
E-mail: pablo.pinacho@uva.es;
E-mail: emiliojose.cocinero@ehu.es;
Web: http://grupodeespectroscopia.es/MW/
[b.] *Instituto Biofisika (CSIC, UPV/EHU), Leioa, 48940, Spain.*
[c.] *Departamento de Química Física y Química Inorgánica, Facultad de Ciencias – I.U. CINQUIMA, Universidad de Valladolid, Paso Belén 7, 47011 Valladolid, Spain.*
Electronic Supplementary Information (ESI) available: [details of any supplementary information available should be included here]. See DOI: 10.1039/x0xx00000x

ideal platform to investigate such systems. The technique delivers rotational constants and nuclear quadrupole coupling data with unrivalled precision, enabling the unambiguous identification of specific conformers, even in the presence of subtle structural differences.[9-13] Small variations in torsion angles or intramolecular hydrogen bonding patterns result in distinct spectral fingerprints, allowing detailed exploration of conformational landscapes.

The advent of broadband chirped-pulse Fourier transform microwave (CP-FTMW) spectroscopy[14,15] has further expanded the scope of these studies. This approach enables the acquisition of rotational spectra over gigahertz-wide frequency windows in a single experiment, facilitating the rapid detection of multiple species and reducing sample consumption. In combination with adiabatic cooling via supersonic expansion,[16] CP-FTMW becomes especially powerful for the analysis of flexible organic molecules, as it strongly favours the observation of only the lowest-energy conformers. This simplifies spectral assignment and enhances sensitivity to weak intramolecular interactions such as hydrogen bonding and dispersive contacts.

After addressing the challenging spectroscopic characterization of DEET,[17] this study presents a comprehensive investigation of the gas-phase structure of picaridin using CP-FTMW spectroscopy, supported by quantum chemical calculations. Emphasis is placed on identifying the dominant conformers for each enantiomeric pair, characterizing their internal geometry, and understanding the role of weak intramolecular forces in shaping the overall structure. Non-covalent interaction (NCI) analysis is employed to dissect the nature of these stabilizing interactions and to elucidate the balance of forces that govern the conformational preferences of this pharmaceutically relevant molecule.

Results and discussion

Conformational space and computational analysis

Picaridin exhibits substantial conformational flexibility due to the length and rotational freedom of its hydroxyethyl and sec-butyl chains attached to the piperidine ring and the carbamate group, respectively. An exhaustive conformational search using B3LYP-D3(BJ)/def2-TZVP with an energy cut-off of 30 kJ·mol^{-1} yielded 142 conformers for the (*R,R*)/(*S,S*) diastereomers and 148 for the (*S,R*)/(*R,S*) pair. To reflect the low-temperature population under supersonic jet conditions, the energy threshold was reduced to 5 kJ·mol^{-1}, retaining only six conformers per diastereomeric family (see Figures S1 and S2; full list of their rotational parameters in Tables S1 and S2).

Within this energy window, all conformers share a common feature: the hydroxyethyl group is locked in place by a strong intramolecular O–H···O hydrogen bond with the carbamate carbonyl oxygen. As a result, the conformational variability observed arises exclusively from the flexibility of the sec-butyl group. This flexibility is defined by the values of two key torsional angles: the δ dihedral angle (C10–C11–C12–C13), which controls the spatial orientation of the terminal ethyl group relative to the methyl group; and the ϕ dihedral angle (C7–O9–C11–C12), which defines the orientation of the entire sec-butyl fragment relative to the molecular backbone (Figure 2). In the most stable conformers of both diastereomeric families, these angles adopt values of approximately δ ≈ 177° and ϕ ≈ 155° (Figure 2), corresponding to an antiperiplanar arrangement of the ethyl and methyl groups and a gauche-like positioning of the sec-butyl chain relative to the ring. As these angles deviate from their optimal values, the energy of the conformers increases gradually: δ shifts from antiperiplanar to synclinal (positive or negative), while ϕ moves from gauche to synclinal or returns to antiperiplanar in the higher-energy species (see Figures S1 and S2). This progression illustrates the delicate energetic balance controlled by side-chain orientation in the conformational space of picaridin.

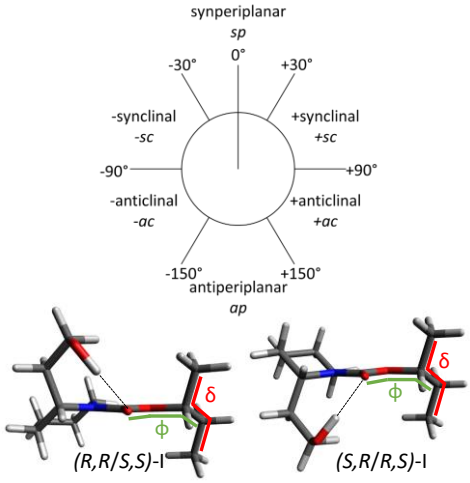

Figure 2. Predicted most stable structures of picaridin (R,R/S,S)-I (left) and (S,R/R,S)-I (right), optimised at the B3LYP-D3(BJ)/def2-TZVP level, showing the orientation of the sec-butyl chains defined by the δ and ϕ dihedral angles.

Rotational spectrum and assignment

The rotational spectrum of picaridin was recorded using chirped-pulse Fourier transform microwave (CP-FTMW) spectroscopy in the 2–6 GHz frequency region under pulsed supersonic expansion conditions. The spectrum revealed two distinct sets of R-branch transitions with well-resolved μ_b-type selection rules, both exhibiting hyperfine structure due to the ^{14}N nuclear quadrupole moment. These two families of transitions were attributed to the most stable conformers of each diastereomeric pair, (*R,R/S,S*)-I and (*S,R/R,S*)-I. The assignment was carried out by fitting the experimental transitions using a semi-rigid rotor Hamiltonian in the I^r representation with Watson's A reduction[18,19] as implemented in SPFIT.[20] The resulting experimental rotational constants, selected centrifugal distortion terms (D_J, D_{JK}, and D_K), ^{14}N quadrupole coupling parameters, dipole moment components, and planar moments of inertia are summarized in Table 1, alongside the values predicted at the B3LYP-D3(BJ)/def2-TZVP level. In the (*R,R/S,S*)-I case, the rotational constants alone were insufficient to unambiguously assign the conformation, as several predicted structures showed nearly indistinguishable values within a few MHz (see Table S1 and Figure S1). However, this can be solved by looking

at the experimental planar moments of inertia, calculated as for example $P_{cc} = (I_a+I_b-I_c)/2$),[¡Error! Marcador no definido.] which are more sensitive to subtle changes in mass distribution. For the (*R,R/S,S*) distereomeric pair, the experimental planar moments of inertia matched only the lowest-energy conformer within the error margin of the fit,confirming the assignment to the (*R,R/S,S*)-I species. In contrast, for the (*S,R/R,S*)-I conformer, the predicted constants were already distinct from those of the other conformers, and both the rotational and planar moments matched the experimental data within 0.5%, providing a more straightforward assignment. For both diastereomers, the sign of D_K differs between experimental and theoretical values (Table 1). This discrepancy may arise from the small magnitude of the constant and its sensitivity to slight variations in the orientation of the alkyl chains. Nevertheless, inclusion of D_K along with D_{JK} was essential to obtain fits with low standard deviation.

Table 1. Experimental and theoretical rotational parameters, dipole moments, and planar moments of inertia for the observed conformers of picaridin. The fits were performed using SPFIT. Theoretical values were computed at the B3LYP-D3(BJ)/def2-TZVP level.

	(*R,R/S,S*)-I		(*S,R/R,S*)-I	
	Theo.	*Exp.*	*Theo.*	*Exp.*
A [MHz][a]	710	710.29926(41)[b]	708	707.60951(57)
B [MHz]	367	368.23132(15)	348	347.89106(15)
C [MHz]	273	273.15095(14)	292	292.00406(19)
D_J [kHz]	0.005	-	0.012	-
D_{JK} [kHz]	0.045	0.1003(92)	0.093	0.156(11)
D_K [kHz]	0.077	-0.070(13)	0.035	-0.194(34)
χ_{aa} [MHz]	2.457	2.1807(16)	2.373	2.2527(18)
χ_{bb} [MHz]	-1.115	-0.9225(82)	-0.726	-0.5255(89)
χ_{cc} [MHz]	-1.341	-1.2581(82)	-1.647	-1.7271(89)
P_{aa} [uÅ²]	1258	1255.56521(58)	1235	1234.60658(70)
P_{bb} [uÅ²]	593	594.61692(58)	496	496.11937(70)
P_{cc} [uÅ²]	119	116.88460(58)	218	218.08670(70)
$\lvert\mu_a\rvert/\lvert\mu_b\rvert/\lvert\mu_c\rvert$ [D]	0.6/3.6/1.9		0.3/4.0/1.5	
N		262		176
σ [kHz]		12.3		12

[a] *A*, *B*, and *C* are the rotational constants; D_J, D_{JK}, and D_K are centrifugal distortion constants; χ_{aa}, χ_{bb}, and χ_{cc} are the ^{14}N nuclear quadrupole coupling constants. P_{aa}, P_{bb}, and P_{cc} are the planar moments of inertia calculated from the moments of inertia (I_a, I_b, and I_c) as for example $P_{cc} = (I_a+I_b-I_c)/2$), $|\mu_a|$, $|\mu_b|$, and $|\mu_c|$ are the absolute values for the dipole-moment component. N is the number of fitted transitions, and σ is the root-mean-square deviation of the fit. [b] Experimental uncertainties are given in parentheses in units of the last digit.

A representative excerpt of the experimental spectrum is reproduced in Figure 3, showing transitions corresponding to both conformers. The fitted transitions reproduce the observed hyperfine splittings with excellent accuracy. The quadrupole coupling constants obtained from the fits are in close agreement with the theoretical predictions, supporting the structural assignment and confirming that the nitrogen atom adopts a pyramidal environment consistent with a substituted piperidine ring. The observed intensities for the rotational transitions for both conformers are also consistent with the predicted values of the dipole moment components, reinforcing the conformational identification. The full list of observed transitions, along with their quantum number assignments and residuals, is provided in Tables S3 and S4.

After assigning all transitions from both conformers, several lines remained unassigned. No additional conformers of picaridin were detected, even after extended signal averaging. Such unassigned lines are commonly observed in CP-FTMW spectra and may originate from impurities, decomposition products, or weakly bound complexes—including adducts with the carrier gas, self-aggregates, or water complexes formed in the expansion. This absence is consistent with low barriers between the lowest-energy structures (Figure S4). In the (*R,R/S,S*) family, the second conformer (designated II) readily interconverts through internal rotation of the ϕ dihedral. For the (*S,R/R,S*) family, the second conformer is essentially isoenergetic with the global minimum, with a relative zero-point corrected energy of 0.5 kJ·mol^{-1}, and a computed barrier for the conversion II→I of only 0.4 kJ·mol^{-1} (Figure S4). Efficient relaxation processes in the core of the supersonic expansion combined with low or negligible barriers (Figure S4), result in rapid conversion to the most stable geometry,[21] explaining why higher energy conformers were not observed in the experimental spectrum. Additional relaxed scans varying either the δ or ϕ dihedral angles were performed to explore possible relaxation pathways among the remaining conformers (Figures S5 and S6). The results indicate feasible relaxation for the conversion of (*S,R/R,S*)-V to (*S,R/R,S*)-III and (*S,R/R,S*)-VI to (*S,R/R,S*)-IV (Figure S6). However, different pathways not explored in this work cannot be rejected as explanations for the absence of the higher-energy conformers. Alternatively, their non-detection could result from the relatively weak signal intensity of the spectrum, which was insufficient even to observe ^{13}C isotopologues.

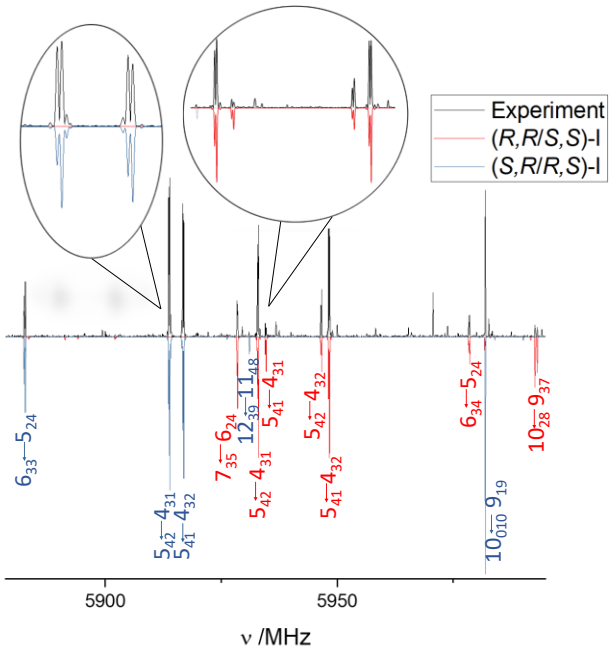

Figure 3. Excerpt of the rotational spectrum of picaridin. The observed trace (black, upward) is shown together with simulated spectra (coloured, downward) for the assigned conformers: (*R,R/S,S*)-I in red, (*S,R/R,S*)-I in blue. Selected transitions are magnified to show the resolved hyperfine structure. A broader frequency range is provided in Figure S3.

Intramolecular interactions

To better understand the stabilization of the experimentally observed conformers, we performed non-covalent interaction (NCI)[22,23] analysis on the optimized geometries of (*R,R/S,S*)-I and (*S,R/R,S*)-I. This method enables visual identification of attractive and repulsive intramolecular contacts based on the topology of the electron density. The resulting NCI isosurfaces are shown in Figure 4, with coloured regions representing the spatial extent and strength of non-covalent interactions. Blue surfaces correspond to attractive interactions with negative values of the second eigenvalue λ_2 of the electron density Hessian matrix, typically associated with hydrogen bonding. Green surfaces indicate weakly attractive dispersion forces ($\lambda_2 \approx 0$), while red surfaces reveal steric repulsion ($\lambda_2 > 0$).

In both conformers, the most prominent interaction is the O–H···O hydrogen bonding between the hydroxyl and the ester carbonyl oxygen, which acts as a structural lock, stabilizing the folded geometry of the hydroxyethyl side chain. As in other carbamates characterized before,[24-26] the carbonyl acts as hydrogen acceptor while the other group, in this case the hydroxyl acts as hydrogen donor. This interaction appears as an intense, localized blue surface between the two atoms involved and is further supported by electron density topology: the bond critical point exhibits a Laplacian $\nabla^2\rho$ with negative curvature and $\lambda_2 < 0$, indicative of strong attraction.

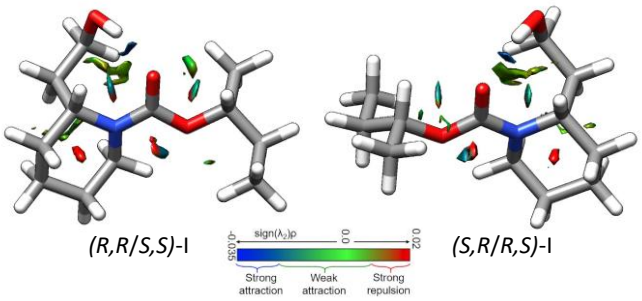

Figure 4. Non-covalent interaction (NCI) plots for the two observed conformers of picaridin: (*R,R/S,S*)-I and (*S,R/R,S*)-I. The sign of λ_2, combined with the electron density, distinguishes the nature of the interactions: attractive (blue/green) and repulsive (red) regions are colour-mapped according to the sign(λ_2)·ρ scale.

Surrounding the ester oxygen, the carbonyl also engages in C–H···O dispersive interactions, particularly with hydrogen atoms on the piperidine ring or the sec-butyl fragment. These interactions are weaker but spatially extended and contribute to the rigidity of the folded geometry. The green isosurfaces in Figure 4 illustrate these dispersion contacts clearly. These interactions, in particular the intramolecular hydrogen bond, play a central role in stabilizing the gas-phase geometry and determining the observable population under supersonic expansion conditions. Importantly, they arise in the absence of any solvent or receptor environment, highlighting their intrinsic nature. In contrast, in the recently reported repellent DEET,[17] conformers are stabilized by weaker dispersion forces, resulting in greater conformational flexibility, which may enable broader but less selective interactions with biological targets compared to the more structurally constrained picaridin.

Structural comparison of assigned conformers

Although (*R,R/S,S*)-I and (*S,R/R,S*)-I are diastereomers stabilized by the same O–H···O hydrogen bond motif, a direct structural comparison reveals subtle but consistent differences. Both conformers adopt a folded geometry stabilized by the intramolecular loop involving the hydroxyethyl and ester groups, and they share nearly identical hydrogen bond distances and angles. However, small deviations appear in the orientation of the sec-butyl fragment. In (*R,R/S,S*)-I, the ϕ dihedral angle is slightly more compressed, leading to a more compact overall shape. This manifests as marginally smaller C rotational constants and planar moments of inertia compared to (*S,R/R,S*)-I, suggesting a slightly tighter mass distribution. These geometric differences, though minor, illustrate how diastereomeric variation can subtly modulate the overall molecular shape even in conformationally locked systems. Such fine structural differences may be relevant in contexts where shape complementarity or stereoselective interactions play a role, for example in binding to chiral receptor sites or membrane environments.

Conclusions

We have studied the structure and conformational preferences of picaridin, one of the most promising candidates to replace DEET[17] as a standard insect repellent. Despite its flexibility and chirality, only one conformer was observed for each diastereomeric pair under gas-phase conditions. These were unambiguously assigned using high-resolution rotational spectroscopy, supported by theoretical predictions of rotational constants, planar moments of inertia, and nuclear quadrupole coupling parameters. Both conformers are stabilised by a strong intramolecular O–H···O hydrogen bond that locks the hydroxyethyl side chain, forming a compact and rigid geometry. Additional dispersion interactions reinforce the structural locking, as revealed by non-covalent interaction analysis.

This work highlights the power of rotational spectroscopy to resolve and characterise individual conformers of flexible, bioactive molecules with exceptional precision. These findings serve as a benchmark for future studies on structure–activity relationships and may aid in the rational design of conformationally constrained repellents.

Methods

Computational methods

A multi-step strategy was used to explore the conformational space of picaridin, following procedures previously applied to flexible systems.[11,27] In the first step, a molecular mechanics conformational search was carried out using the Merck Molecular Force Field (MMFFs)[28] as implemented in Macromodel version 14 release 2024-4.[29] This force field is parametrised for a wide range of organic functional groups and is well-suited to modelling the flexibility of

molecules such as picaridin. Picaridin has four stereoisomers grouped into two enantiomeric pairs: (*R,R*)/(*S,S*) and (*S,R*)/(*R,S*). Since enantiomers are mirror images and share identical rotational constants, they cannot be distinguished under the conditions of our experiment. For this reason, the conformational search was restricted to one representative of each pair: (*R,R/S,S*) and (*S,R/R,S*).

The resulting geometries were subsequently reoptimised using quantum mechanical calculations at the B3LYP-D3(BJ)/def2-TZVP level.[30-32] Harmonic frequency analysis was performed to confirm the nature of the stationary points and to obtain zero-point corrected energies. All quantum chemical calculations were carried out using the Gaussian16 software package revision A.03.[33] Theoretical rotational parameters and relative energies for all conformers within each diastereomeric family are listed in Tables S1 and S2 of the Supplementary Information.

Experimental methods

A commercial sample of picaridin (95% purity) was used without further purification. The rotational spectrum was recorded using the chirped-pulse Fourier-transform microwave (CP-FTMW) spectrometer developed at the University of the Basque Country[15,34] based on the original broadband designs.[14] The sample, a colourless liquid at room temperature, was heated to 150 °C to generate a sufficient vapour pressure. The vapour was seeded in neon at a backing pressure of 2 bar and introduced into the vacuum chamber through a pulsed solenoid valve operating at 1 Hz. A 4 μs excitation pulse was applied to induce macroscopic polarisation, followed by a short delay and acquisition of a 20 μs free induction decay (FID) signal. Ten excitation–detection cycles were performed per gas pulse, yielding an effective repetition rate of 10 *Hz*. A total of 1,400,000 FIDs were co-added to produce the final broadband spectrum.

Conflict of interest

The authors declare no conflicts of interest.

Author contributions

Otger Crehuet: conceptualization, investigation, formal analysis, writing – first draft, writing – review and editing. Andrea Vázquez: formal analysis, writing – review and editing. Francisco J. Basterretxea: funding acquisition, project administration, writing – review and editing. Pablo Pinacho: formal analysis, writing – review and editing. Emilio J. Cocinero: conceptualization, funding acquisition, project administration, writing – review and editing.

Acknowledgments

E.J.C. and F.J.B. acknowledge financial support from the Spanish Ministry of Science and Innovation (MCIN/AEI, Project PID2023-147698NB-I00) and the Basque Government (Project IT1491-22). P. P. acknowledges a Maria Zambrano grant (UPV/EHU, Ministry of Universities, Recovery, Transformation, and Resilience Plan – Funded by the European Union – Next Generation EU, MAZAM22/16). The authors also acknowledge the use of computational resources provided by SGIker (UPV/EHU) and CESGA.

References

[1] T. M. Katz, J. H. Miller, A. A. Hebert, *J. Am. Acad. Dermatol.*, **2008**, *58*, 865-871.
[2] M. Londershausen, *Pestic. Sci.*, **1996**, 48, 269-292.
[3] E. T. Mccabe, W. F. Barthel, S. I. Gertler, S.A. Hall, *J. Org. Chem.*, **1954**, *19*, 493–498.
[4] G. Paluch, L. Bartholomay, J. Coats, *Pest. Manag. Sci.,* **2010**, *66*, 925-935.
[5] B. V. Travis, F. A. Morton, H. A. Jones, J. H. Robinson, *J. Econ. Entomol.*, **1949**, 42, 4, 686–694.
[6] J. Boeckh, H. Breer, M. Geier, F. P. Hoever, B. W. Kriiger, G. Nentwig H. Sass, *Pestic. Sci*., **1996**, 48, 359-373.
[7] N. P. Charlton, L. T. Murphy, J. L. Parker Cote, J. P. Vakkalanka, *Clin. Toxicol.* **2016**, *54,* 655-658.
[8] R. Natarajan, S. C. Basak, A. T. Balaban, J. A. Klun, W. F. Schmidt, *Pest. Manag. Sci.,* **2005**, *61*, 1193-1201.
[9] N. A. Seifert, I. A. Finneran, C. Pérez, D. P. Zaleski, J. L. Neill, A. L. Steber, R. D. Suenram, A. Lesarri, S. T. Shipman, B. H. Pate, *J. Mol. Spectrosc.*, **2015**, *312*, 13-21.
[10] S. R. Domingos, C. Pérez, C. Medcraft, P. Pinacho, M. Schnell, *Phys. Chem. Chem. Phys.*, **2016**, 18**,** 16682-16689.
[11] I. Uriarte, S. Melandri, A. Maris, C. Calabrese, E. J. Cocinero, *J. Phys. Chem. Lett.*, **2018**, *9,* 1497–1502.
[12] V. W. Y. Tsoi, E. Burevschi, S. Saxena, M. E. Sanz, *J. Phys. Chem. A*, **2022**, *126*, 6185–6193.
[13] A. N. Mort, F. Xie, A. S. Hazrah, Y. Xu, *Phys. Chem. Chem. Phys.*, **2023**, *25*, 16264-16272.
[14] G. Brown, B. C. Dian, K. O. Douglass, S. M. Geyer, S. T. Shipman, B. H. Pate, *Rev. Sci. Instrum,* **2008**, *79*, 053103.
[15] I. Uriarte, P. Écija, L. Spada, E. Zabalza, A. Lesarri, F. J. Basterretxea, J. A. Fernández, W. Caminati, E. J. Cocinero, *Phys. Chem. Chem. Phys*, **2016**, *18*, 3966–3974.
[16] D. H. Levy, *Science*, **1981**, 214, 263-269.
[17] O. Crehuet, A. Vázquez, P. Pinacho, A. Insausti, E. R. Alonso, F. J. Basterretxea, E. J. Cocinero, *Phys. Chem. Chem. Phys.*, **2024**, *26*, 24455-24460.
[18] W. Gordy and R. L. Cook, *Microwave Molecular Spectra*, Wiley, **1984**, New York**.**
[19] J. K. G. Watson, *Vibrational Spectra and Structure a Series of Advances*, Elsevier, Amsterdam, **1977**.
[20] H. M. Pickett, *J. Mol. Spectrosc.,* **1991**, *148*, 371–377.
[21] R. S. Ruoff, T. D. Klots, T. Emilsson, H. S. J. Gutowsky, *Chem. Phys.,* **1990**, *93*, 3142-3150.
[22] E. R. Johnson, S. Keinan, P. Mori-Sánchez, J. Contreras García, A. J. Cohen, W. Yang, *J. Am. Chem. Soc.*, **2010**, *132, 6498–6506*.
[23] J. Contreras-García, E. R. Johnson, S. Keinan, R. Chaudret, J. P. Piquemal, D. N. Beratan, W. Yang, *J. Chem. Theory Comput.*, **2011**, *7, 625–632.*
[24] P. Pinacho, J. C. López, Z. Kisiel, S. Blanco, *J. Phys. Chem. A*, 2019, ***123***, 7983–7990.

[25] P. Pinacho, J. C. López, Z. Kisiel, S. Blanco, *Phys. Chem. Chem. Phys.*, **2020**, *22*, 18351-18360.
[26] P. Pinacho, J. C. López, Z. Kisiel, S. Blanco, *J. Chem. Phys.,* **2024**, *160*, 164315.
[27] C. Calabrese, I. Uriarte, A. Insausti, M. Vallejo-López, F. J. Basterretxea, S. A. Cochrane, B. G. Davis, F. Corzana, E. J. Cocinero, *ACS Cent. Sci.* **2020**, 6, *293–303*.
[28] T. A. Halgren, *J. Comput. Chem.*, **1996**, *17*, 553-586.
[29] F. Mohamadi, N. G. J. Richards, W. C. Guida, R. Liskamp, M. Lipton, C. Caufield, G. Chang, T. Hendrickson, W. C. Still, *J. Comput. Chem.*, **1990,** *11*, 440-467.
[30] A. D. Becke, *J. Chem. Phys,* **1993**, *98*, 5648–5652.
[31] F. Weigend, R. Ahlrichs, *Phys. Chem. Chem. Phys.*, **2005**, *7*, 3297-3305.
[32] S. Grime, A. Jens, E. Stephan, H. Krieg, *J. Chem. Phys*, **2010**, *132*, 154104
[33] Gaussian 16, Revision A.03, M. J. Frisch, G. W. Trucks, H. B. Schlegel, G. E. Scuseria, M. A. Robb, J. R. Cheeseman, G. Scalmani, V. Barone, G. A. Petersson, H. Nakatsuji, X. Li, M. Caricato, A. V. Marenich, J. Bloino, B. G. Janesko, R. Gomperts, B. Mennucci, H. P. Hratchian, J. V. Ortiz, A. F. Izmaylov, J. L. Sonnenberg, D. Williams-Young, F. Ding, F. Lipparini, F. Egidi, J. Goings, B. Peng, A. Petrone, T. Henderson, D. Ranasinghe, V. G. Zakrzewski, J. Gao, N. Rega, G. Zheng, W. Liang, M. Hada, M. Ehara, K. Toyota, R. Fukuda, J. Hasegawa, M. Ishida, T. Nakajima, Y. Honda, O. Kitao, H. Nakai, T. Vreven, K. Throssell, J. A. Montgomery, Jr., J. E. Peralta, F. Ogliaro, M. J. Bearpark, J. J. Heyd, E. N. Brothers, K. N. Kudin, V. N. Staroverov, T. A. Keith, R. Kobayashi, J. Normand, K. Raghavachari, A. P. Rendell, J. C. Burant, S. S. Iyengar, J. Tomasi, M. Cossi, J. M. Millam, M. Klene, C. Adamo, R. Cammi, J. W. Ochterski, R. L. Martin, K. Morokuma, O. Farkas, J. B. Foresman, and D. J. Fox, Gaussian, Inc., Wallingford CT, 2016.
[34] I. Uriarte, C. Pérez, E. Caballero-Mancebo, F. J. Basterretxea, A. Lesarri, J. A. Fernández, E. J. Cocinero, *Chem. Eur. J.,* **2017**, *23*, 7238-7244

